Journal of Computational Applied Mechanics 2023, 54(4): 533-551

DOI: 10.22059/JCAMECH.2023.363102.857

RESEARCH PAPER

Exploring Optimal Configurations for a Wind Farm with Clusters of Darrieus VAWT, Using CFD Methodology

Farzad Ghafoorian[a], Seyed Reza Mirmotahari [b], Farnaz Bakhtiari [b], Mehdi Mehrpooya [c,*]

[a] *Turbomachinery Research Laboratory, Department of Energy Conversion, School of Mechanical Engineering, Iran University of Science and Technology, Tehran, Iran.*

[b] *Hydrogen and fuel cell laboratory, Faculty of New Sciences and Technologies, University of Tehran, Tehran, Iran.*

[c] *Renewable Energies and Environment Department, Faculty of New Sciences and Technologies, University of Tehran, Tehran, Iran.*

Abstract

Due to the alarming increase in greenhouse gases, switching to clean, renewable energy sources like wind energy has become imperative. As a result, the use of different wind turbines to generate electricity increased worldwide. Meanwhile, Darrieus vertical axis wind turbines (VAWTs) have gained considerable popularity due to their acceptable efficiency. Individual wind turbines are not efficient enough for widespread use and are only suitable for providing domestic energy; therefore, they should be placed in the form of turbine clusters in wind farms. The wind farm configuration and cluster placement have specific considerations, including the rotors' optimal installation distance and rotational direction. In the present study, the rotors installation distance in an array including a cluster of three Darrieus rotors is investigated, and the CFD and Kriging optimization results ensured that the best installation distance is equal to 1.5 times the diameter (1.5D). Also, the CFD results for the rotor's rotational direction at the installation distance of 1.5D showed that when the lower downstream rotor is counter-rotating the leading rotor and clockwise, the overall efficiency of the cluster increases by 67.1%. Additionally, two V-shaped and rhombic configurations are modeled, and the overall efficiency of each turbine in two different configurations is compared separately with the single turbine. In the optimum case, the overall efficiency of turbine A in the V-shaped configuration of three turbines and the rhombic configuration of 12 turbines improved by 54% and 36%, respectively, compared to the single turbine. The study of the streamlines showed that the main reason for improving the performance in the V-shaped configuration is the favorable velocity gradient around the blade, and the decrease in overall efficiency in the V-shaped and rhomboid configurations is wake flow intensity and trapping between the rotors which cause the stagnation zone.

Keywords: Darrieus VAWT; Darrieus VAWT cluster; Wind farm simulation; CFD simulation of turbulent flow;

1. Nomenclature

V_∞	Inlet flow velocity (m/s)
n	Rotational speed (rpm)
T	Torque (N.m)
P	Output power (W)
R	Rotor radius (m)
X	Lateral distance (m)

* Corresponding author. *E-mail address:* mehrpoya@ut.ac.ir (M. Mehrpooya).

Y	Vertical distance (m)
C_p	Power coefficient
t	Turbulence
μ	Viscosity (Pa.s)
ω	Angular velocity (rad/s)
ρ	Density (kg/m3)
VAWT	Vertical axis wind turbine
HAWT	Horizontal axis wind turbine
CFD	Computational fluid dynamic
TSR	Tip speed ratio
URANS	Unsteady Reynolds averaged Naiver Stokes

2. Introduction

The unacceptable growing rate of greenhouse gases and the cost of old-fashioned fossil fuels led to an increase in utilizing renewable energy sources like wind, solar, geothermal, and biomass energy. Wind energy is considered one of the most reliable renewable energy sources; therefore, it causes a remarkable increase in wind farm development all around the world [1]. Also, power plants based on renewable energy can work in the form of combined cycles and be useful in various industries, such as water desalination plants [2]. Wind turbines can be classified based on their rotation axis into two groups including, Horizontal Axis Wind turbines (HAWTs) and Vertical Axis Wind Turbines (VAWTs) [3]. VAWTs have several advantages compared to HAWTs, namely lower installation and maintenance costs, independence from the wind flow direction, and fewer mechanical devices [4]. VAWTs are categorized based on their rotational force into two types; the first group is drag-based turbines like Savonius VAWTs, which are old-fashioned rotors that can operate as shallow water wells pumps [5]. The second category is lift-based rotors, and they operate with the help of lift forces like Darrieus and Gorlov VAWTs. These VAWTs' power output is significantly more than Savonius turbines; however, they need initial torque to start rotation [6]. In order to solve the mentioned disadvantage, a drag-based rotor can be combined with a lift-based rotor so the initial torque can be prepared [7]. Also, installing wind turbines individually for mass production of energy is not cost-effective; as a result, turbines are installed in clusters or wind farms with different arrangements. Obviously, the researcher's motivation is to find an optimal structure for installing wind turbines [8]. The importance of the optimal design of wind farms first showed itself in the arrangement of HAWTs. For example, the cone-shaped pattern of antlion hunting activity was used for the effective installation layout of HAWTs [9]. For the VAWTs cluster installation, the turbine rotors' installation distance and the rotation direction relative to the prevailing wind flow are particularly important [10]. The results of CFD simulations have shown that the wake flow in the downstream section of the rotor affects the rear turbine performance. This wake flow can have favorable or unfavourable effects depending on the distance between the turbines [11]. In fact, it can be claimed that the analysis of the downstream turbine wake flow and its effects on the leading and trailing turbines, which is dependent on the distance and angle of the rotor installation and the direction of rotation of the rotors, is the essential element in the wind farms design [12]. Usually, to evaluate the optimal distance, a ratio between the rotor diameter and the distance between the rotors is defined as the normalized distance. The results show that the performance of the pioneering turbine decreases at a small normalized distance [13]. It should also be noted that the mutual interaction phenomenon reduces the Cp of the rear turbines at very small normalized distances, i.e., the distance is less than the diameter of the rotor [14]. On the other hand, at close distances, there is a chance to reuse the wake flow energy, which, with the help of this phenomenon, at an optimal distance of about 1.5 times the rotor diameter, the maximum Cp from the wind farm was obtained [15]. Meanwhile, the arrangement of turbine clusters is also discussed. The results show that the staggered triangle arrangement when two turbines are placed upstream has the highest efficiency [16]. The results of an experimental study proved that in addition to the minimum installation downstream turbine distance, which increases the pioneer turbine efficiency compared to the single turbine case, the installation angle also remarkably affects the system performance [17]. According to CFD results, 45° installation increases the Cp for the upstream turbine, while 150° increases the efficiency of the downstream turbines [18]. It should be noted that the wake flows behind the turbines and its effects on the upstream turbine performance depend on the TSR and wind speed in addition to the installation angle and distance [19]. Rotational direction plays a vital role in the VAWT cluster. To achieve a higher Cp value for the upstream turbine, downstream turbines or one of them are considered counter-rotating rotors [20]. The streamlines and vortices flow study showed that the wake flow of counter-rotating downstream turbines could improve the VAWT cluster's overall performance at optimum installation distance [21]. In the last step of wind farm numerical modeling, the design parameters like distance and installation angle should be optimized by a practical optimization approach like the Kriging method or genetic algorithm to find the best

layout [22]. It should be noted that in addition to optimization, sensitivity analysis is another important step to determine which of the design parameters has the most effect on the system's output response; in other words, it shows the dependence of the responses on each of the parameters [23]. Different optimization methods, such as the Design of Experiments method (DOE), in which the Response Surface Method (RSM) is one of its subsets, have always helped to optimize CFD modeling results. The RSM approach is based on two common methods, namely Central Composite Design (CCD) and Box-Behnken Design (BBD) [24, 25] .

Based on the literature review, the main objective of this study is the cluster optimization of Darrieus VAWTs. To achieve this goal, a V-shaped array of Darrieus vertical axis wind turbines is considered the initial design for CFD simulation; this configuration is inspired by a migratory bird model. The overall Cp values are considered the main criteria for evaluating the efficiency of the wind farm and Darrieus VAWT clusters. They are evaluated for different installation distances, which means the vertical and lateral distances increase gradually and with a regular pattern. Subsequently, after finding the optimal installation distance with the Kriging optimization approach and designing different experiments for the lateral and vertical distances, the rotational direction of the rotors is evaluated for both clockwise (CW) and counter-clockwise (CCW) cases for the optimal distance and the most effective rotational direction are obtained. In the last stage, after a complete examination of clusters with three Darrieus VAWT, a V-shaped configuration with three, five, and seven Darrieus VAWT clusters, and a novel rhombic configuration with four, eight, and twelve Darrieus VAWTs at the optimal installation distance and rotational direction condition is simulated. The general purpose of presenting the novel rhombus configuration model is to study more closely the effect of the wake flow behind the upstream turbines on the performance of the downstream turbines, and the general performance of the conventional V-shaped layout that has an open end is compared with this new design.

3. Problem description and geometry configuration

A 2D CFD investigation is conducted to identify the optimized Darrieus VAWT cluster in a V-shaped configuration in order to find a productive wind farm layout. The main reason for choosing a two-dimensional solution is to simplify the problem and reduce computational costs. Obviously, this model has some shortcomings. However, it is sufficient for modelling the wake flow behind the turbine and blades and streamlines, which are the dominant phenomena in this modelling, and their effects should be investigated. Also, as the Darrieus rotor is H-rotor VAWT and consists of straight blades, in 2D simulation, the blades can be assumed as airfoil profile spanwise, and the physics of flow around the airfoil spanwise follow the flow behaviour around straight blades. Due to migrating geese's tendency to fly in a V-shape arrangement, as can be seen in Fig. 1(a), the rotors were located in a V-shaped layout. Downstream geese fly in updrafts and benefit from pressure differential to protect their energy, as the goose in the upstream section creates high-velocity airflow in the wake regime zone. Similarly, upstream rotors make a lengthy wake regime with a sporadic high-velocity zone on each side. The high-velocity area and the velocity differential can be used to enhance the downstream turbines by installing them in optimum positions. Also, downstream turbines' optimum distance can improve the leading rotor by wake energy reuse. As can be seen from Fig. 1 (b), the upstream turbine and both lower and upper downstream turbines with counter-clockwise rotational direction are turbines A, B, and C, respectively. The installation distance between the turbines B and A axis of rotation is considered as (XB, YB). Similarly, this value between the rotational axis of turbines C and A is named (XC, YC). The positions of turbines B and C are evaluated at four different vertical and lateral distances. Downstream turbines are spaced from 1.5D to 3D with 0.5m vertical and lateral intervals.

The dimensions of the single turbine, which is also known as the leading turbine, have been extracted from the experimental study of M. Raciti Castelli et al. [26]. This numerical study considers a rectangle as the stator or wind tunnel test section. The turbine rotor dimensions, geometrical specifications, and stator are addressed in Table: 1, and its schematic is presented in Fig. 2.

As can be seen from Figure 2, in order to increase the accuracy of the results, blades are divided into sub-domains. Also, the length and width of the rotor are far enough from the rotor zone to allow fluid flow to complete development. To simplify the CFD calculations, the shafts and supporting arms of the blades have been omitted from the geometry.

4. Governing equations

In this section, the equations governing fluid flow are described. Governing equations for turbulent flow modeling and fluid mechanics equations will be discussed. Then, mathematical relationships for data extraction, including output power and model optimization, will be presented.

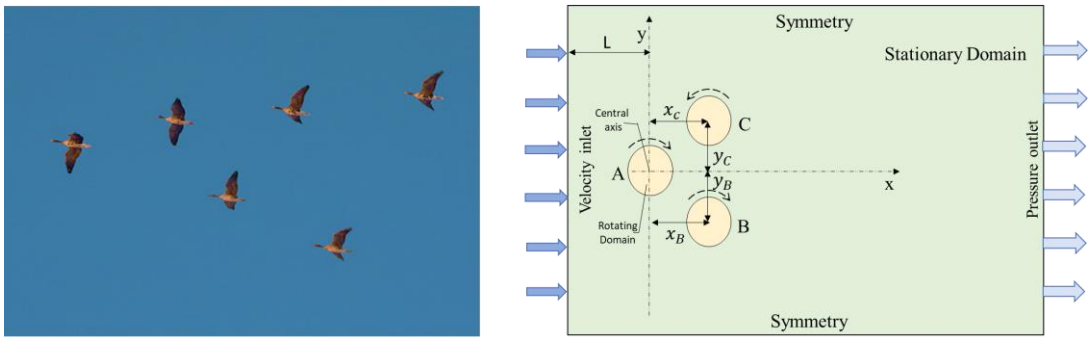

(a) (b)

Fig. 1 (a) Migrating geese, (b) V-shaped layout [27]

Table: 1Dimensions and main geometric characteristics of the simulated turbine rotor and stator.

Quantity	Value
Number of blades	3
Profile of blade	NACA0021
Length of chord	0.0858(m)
Radius of rotor	0.515(m)
Solidity of rotor	0.5
Height of blade	1(2D simulation)
Length of stator	25(m)
Width of stator	4(m)

4.1. Turbulence Modeling

The ongoing CFD simulation involves numerical modeling based on incompressible, viscous Navier-Stokes mathematical equations, which simulate fluid flow across the rotor. Equation 1 provides two terms, $\bar{u}$ and u' that determine the velocity [28].

$$u' = u - \bar{u} \tag{1}$$

In the given equation, the symbol ($\bar{u}$) represents the time-averaged mean flow velocity, while (u') denotes the fluctuating velocity elements. Equation 2 displays the time-averaged mean flow velocity [28].

$$\bar{u} = \frac{1}{T}\int_T u(t)dt \tag{2}$$

Continuity and momentum equations of URANS are defined by equations 3 and 4, respectively [29].

$$\frac{\partial \overline{u_i}}{\partial x_i} = 0 \tag{3}$$

$$\frac{\partial \overline{u_i}}{\partial t} + \overline{u_j} \frac{\partial u_i}{\partial x_j} = -\frac{1}{\rho} \frac{\partial \overline{p}}{\partial x_i} + \nu \frac{\partial^2 \overline{u_i}}{\partial^2 x_j^2} - \overline{u_j' \frac{\partial u_i'}{\partial x_j}} \tag{4}$$

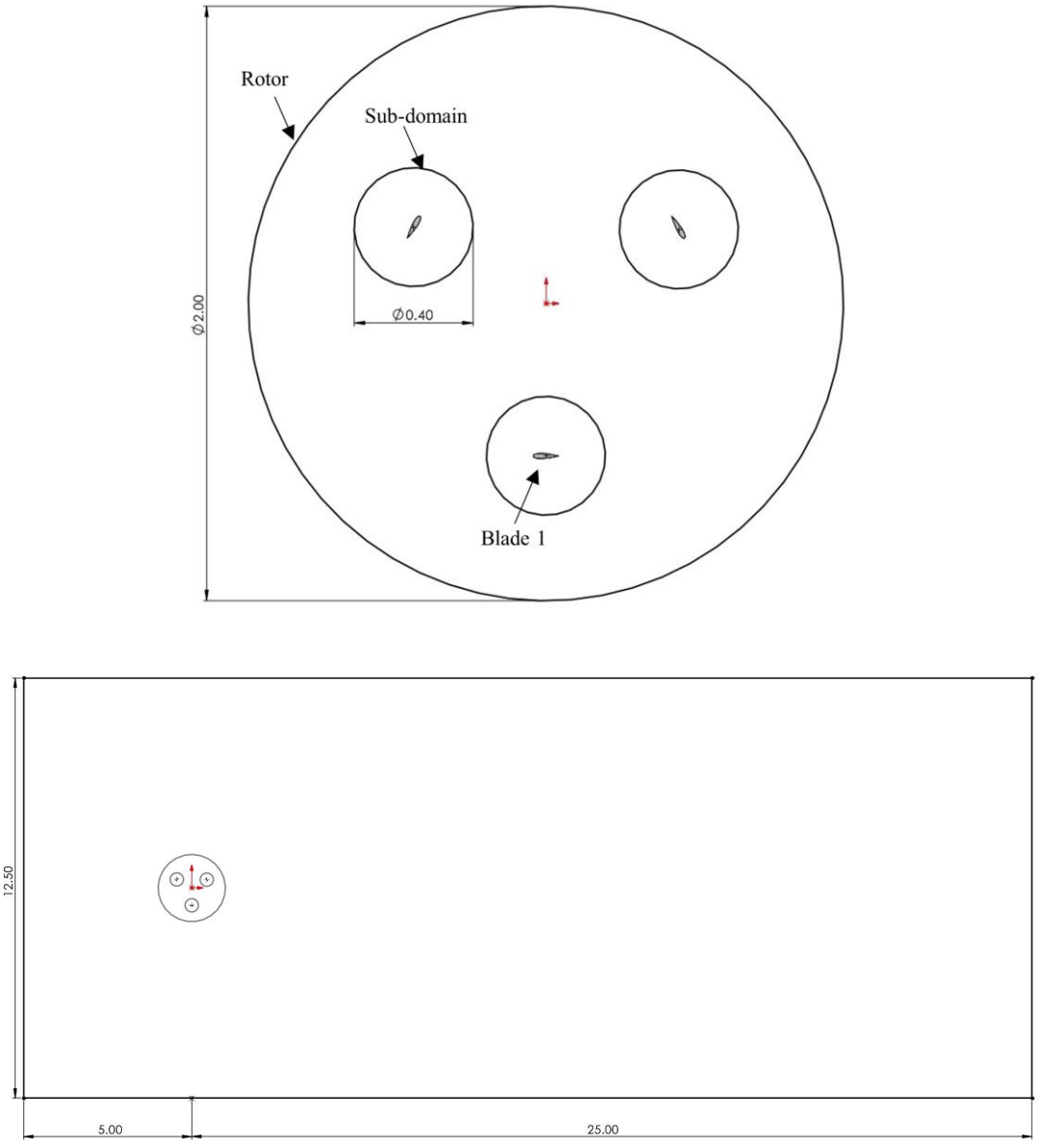

Fig. 2 Schematic of the 3-bladed Darrieus turbine with dimensions.

In the above equations, u is defined as the fluid flow velocity (m/s), p is pressure (Pa), and ρ (kg/m3) is the fluid density.

Standard equation turbulence models are commonly used in CFD simulations to analyse turbulent flow, such as the k-ε and k-ω models. The former is suitable for free-shear layer flow far from wall domains with low-pressure gradients, while the latter predicts turbulence in the boundary layer sub-layer and is used near surfaces. For accurate

forecasting of the aerodynamic performance of Darrieus rotors at low Reynolds numbers, where stall occurrence is crucial, the SST k-ω model combines both approaches. This model solves the transport mathematical relation for both turbulent kinetic energy (k) and turbulent specific dissipation rate (ω) while also calculating the specific turbulent dissipation to determine the turbulent length scale [29]. The governing equations for the SST k-ω model are listed below [30].

$$\frac{\partial k}{\partial t}+U_i\frac{\partial k}{\partial x_i}=\frac{\partial}{\partial x_i}\left[\left(\nu+\sigma_k\nu_t\right)\frac{\partial k}{\partial x_i}\right]+P_k-C_\mu\omega k \tag{5}$$

$$\frac{\partial \omega}{\partial t}+U_i\frac{\partial \omega}{\partial x_i}=\frac{\partial}{\partial x_i}\left[\left(\nu+\sigma_\omega\nu_t\right)\frac{\partial \omega}{\partial x_i}\right]+\gamma\frac{\omega}{k}P_k-\beta\omega^2+(1-F_1)\frac{2\sigma_\omega}{\omega}\frac{\partial k}{\partial x_i}\frac{\partial \omega}{\partial x_i} \tag{6}$$

The transport coefficients are combined versions of two models. The combined function F_1 is [31]:

$$F_1=\tanh(\arg_1^4) \tag{7}$$

Where

$$\arg_1=\min[\max\left(\frac{\sqrt{k}}{C_\mu\omega y},\frac{500\nu}{y^2\omega}\right),\frac{4\rho\sigma_{\omega^2}k}{CD_{k\omega}y^2}] \tag{8}$$

In the equation, y is defined as the normal distance to the wall, and $CD_{k\omega}$ is the positive term of the cross-diffusion relation:

$$CD_{k\omega}=\max\left(2\rho\sigma_{\omega^2}\frac{1}{\omega}\frac{\partial k}{\partial x_i}\frac{\partial \omega}{\partial x_i},10^{-20}\right) \tag{9}$$

Based on the SST model, the eddy viscosity is calculated by:

$$\nu_t=\frac{a_1k}{\max(a_1\omega,\Omega F_2)} \tag{10}$$

Where Ω defined as the vorticity vector magnitude and the coefficient F_2 is determined by the below equation: Here Ω is the vorticity vector magnitude. The coefficient F_2 is calculated by the following equation:

$$F_2=\tanh(\arg_2^2) \tag{11}$$

Where

$$\arg_2=\max\left(\frac{2\sqrt{k}}{C_\mu\omega},\frac{500\nu}{y^2\omega}\right) \tag{12}$$

SST model constants are 0.09 and 0.31, respectively.

4.2. Mathematical equations

Tip speed ratio (TSR), which is an important element of turbine performance, is introduced by the relation between the blade leading edge rotational velocity and the free stream velocity as follows [31]:

$$TSR=\frac{R\times\omega}{V_{in}} \tag{13}$$

Another dimensionless parameter is the power coefficient (C_p), which is defined as the relation between the maximum output power and the kinetic energy flux value passing the rotor leading area, and it can be determined as below [32].

$$C_P=\frac{P}{\frac{1}{2}\rho AV_\infty^3} \tag{14}$$

The output power (P) is achieved from overall torque (T) around the rotor vertical axis times to the angular velocity. Also, ρ (kg/m^3) is the air density, V_∞(m/s) is the wind flow velocity, and A (m^2) is the rotor-swept area.

4.3. Kriging optimization formulation

The Kriging approach is employed to generate the surrogate algorithm through a variety of modifications to the layout's location. The relation between the target C_p and the position is represented by the Kriging method. The highest value of C_p presents the downstream rotor's optimum arrangement location (x, y). The unidentified function y^ is introduced using the Kriging method:

$$\hat{y} = \beta + z(X) \tag{15}$$

X is defined as a two-dimensional vector, β and $z(X)$ are the linear regression term and the local deviation, respectively. Gaussian model and stationary random process with zero mean and covariance is represented by z(X):

$$E[z(X)] = 0 \tag{16}$$

$$Var[z(X)] = \sigma^2 \tag{17}$$

$$E[z(X)z(X_i)] = \sigma^2 R(X, X_i) \tag{18}$$

σ^2 is defined as stationary random process variance; $R(X, X_i)$ is the spatial correlation function, which indicates the correlation between $z(X)$ and $z(X_i)$. The Spatial Correlation Function (SCF) is defined as [32]:

$$R(X, X_i) = \exp\left[-\sum_{i=1}^{n} \theta_k (X_{ki} - X_k)^2\right] \tag{19}$$

θ_k is named as k*th* term of the correlation vector parameter θ. The correlation matrix can be defined as below:

$$R = \begin{bmatrix} R(X_1, X_1) & \cdots & R(X_1, X_N) \\ \vdots & \ddots & \vdots \\ R(X_N, X_1) & \cdots & R(X_N, X_N) \end{bmatrix} \tag{17}$$

Each simple point can be combined in various ways, and these combinations are represented by matrix *R*. The correlation between an unknown prediction point *X* and *N* sample points is defined as follows.

$$r(X) = \begin{bmatrix} R(X, X_1) \\ \vdots \\ R(X, X_N) \end{bmatrix} \tag{18}$$

The final Kriging approach predictor $\hat{y}$ is as follows:

$$y = \beta + r^T(X) R^{-1} (Y - E(g(X)) \tag{19}$$

In the above equation, $\hat{\beta}$ is the least-squares estimated of β; Y is the N-dimensional vector:

$$\beta = (E^T R^{-1} E)^{-1} E^T R^{-1} Y \tag{20}$$

$$Y = \{y(X_1) y(X_2) \ldots y(X_N)\}^T \tag{21}$$

The Kriging predictor's uncertainty $\hat{y}$(X) is shown as follows:

$$MSE = E\left[\left(y(X) - y(X)\right)^2\right] = \sigma^2 \left\{1 - r^T(X) R^{-1} r(X) + \left[1 - E^T R^{-1} r(X)\right]^2 \left(E^T R^{-1}\right)^{-1}\right\} \tag{22}$$

The mean squared error of $y(X)$ is reported by MSE.

5. Numerical modelling and solution strategy

In this section, the structure and method of meshing are explained, and the boundary and operational conditions are described. According to the numerical setup for a single Darrieus VAWT, the validation is compared to the previous experimental results and the study of the mesh to check its quality and the independence of the solution from the number of elements placed.

5.1. Grid Structure Description

ANSYS Meshing application was selected for the current numerical modelling discretizing. Since Darrieus VAWT blades do not have a helical angle, a 2D model is acceptable and considered for mesh generation, which means the meshing technique is similar to the common techniques for simple spanwise airfoil profile meshing. An

unstructured approach with an all-triangular perspective was used for gridding all domains containing stator, rotor, and sub-domains. To improve and enhance the accuracy of the CFD results around the interfaces and rotor blades, suitable sizing was done. Also, for more precise CFD outputs and to capture the effects of flow separation near the blade walls, especially near the leading and trailing edge, an acceptable mesh size and inflation mesh, which contains 12 layers with a growth factor of 1.1, were adopted. By considering these values and methods, the desired value of y+<1 can be reached. Mesh is shown in Fig. 3.

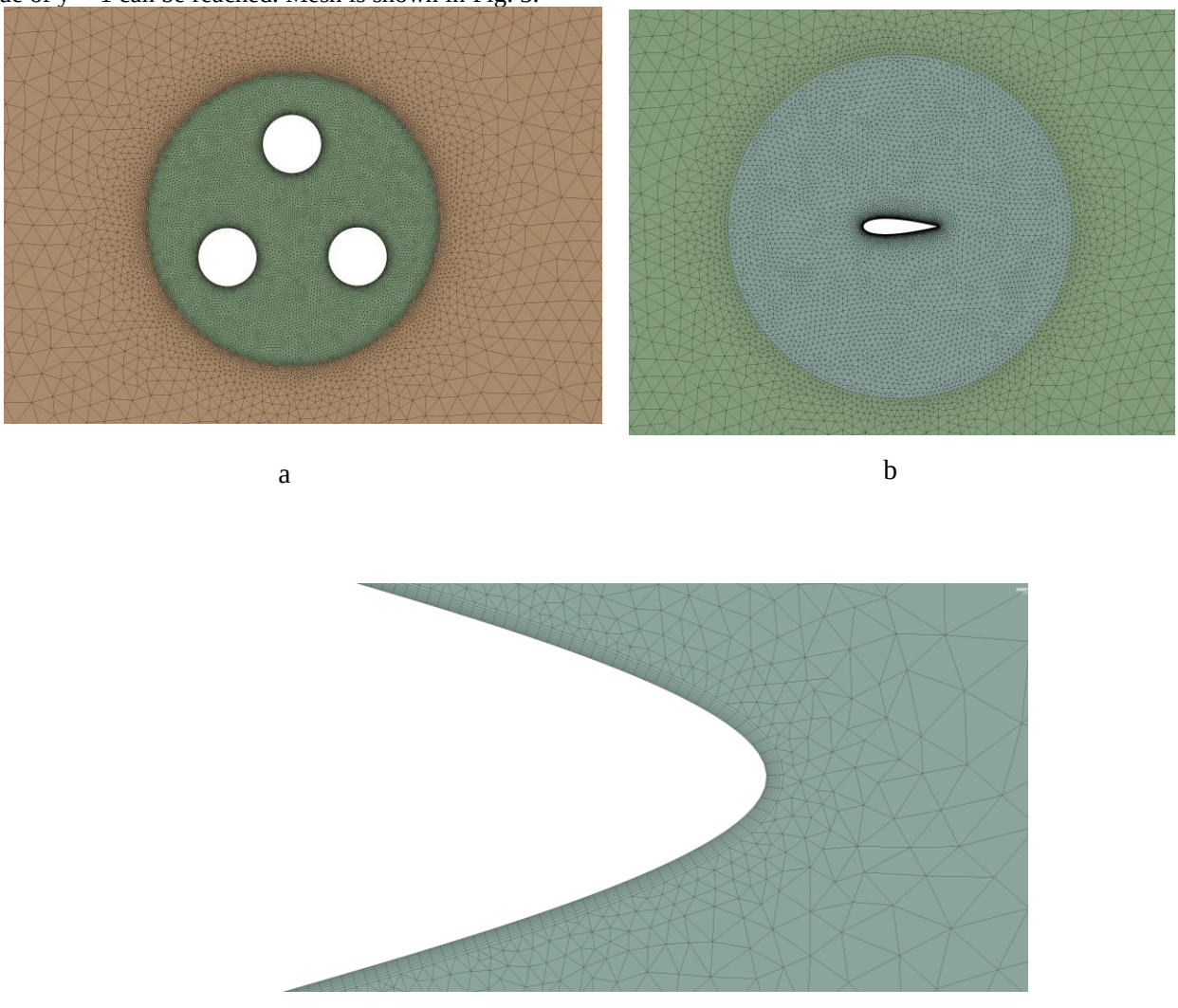

a b c

Fig. 3 a) Rotor mesh, b) Sub-domain mesh, and c) Airfoil boundary layers and mesh.

5.2. Boundary condition and solver setting

The current 2D CFD investigation was conducted on Ansys Fluent. Based on the unsteady physics of the problem, the transient approach was selected to simulate Fluid flow movement between the rotor blades and around the leading and trailing edges. The no-slip condition assumption is considered for the blades' edges. The stator upstream zone is considered the velocity inlet boundary condition, and the inlet wind velocity value is 9(m/s) with moderate turbulence intensity. Based on the rotor geometry and considered inlet wind velocity, the Reynolds number is equal to 630000, which indicates this turbine is working in the low Reynolds number range; however, the flow regime is turbulent. In other words, the wind flows uniformly and at a constant value over time, perpendicular to the rotor rotational axis. The stator downstream section is set as a pressure outlet boundary condition with 1atm static pressure. The Left and right sides of the stator are considered walls, and they do not have any significant effect on simulation outputs as they are far from the rotor domain. A fluid-fluid interface condition is defined around the

rotor, and this surface is well coupled to the stator region in order to model the rotational motion of the turbine. A similar boundary condition has been assumed for the sub-domains, with the difference that they do not have absolute motion and have rotational motion relative to the main rotor. To ensure accuracy, we have set the convergence standard to a residual value of 10-6. We've also opted for a high-resolution advection scheme and a second-order backward Euler for the transient scheme. The time step size is fixed at 0.001 seconds.

5.3. Model validation and Mesh analysis

A three-bladed Darrieus VAWT experimental output which conducted by Castelli et al [27]. Was selected to validate the current CFD investigation. According to experimental modelling outputs, the C_p was evaluated in four different TSRs. A comparison of experimental results and CFD results obtained for validation is given in Fig. 4.

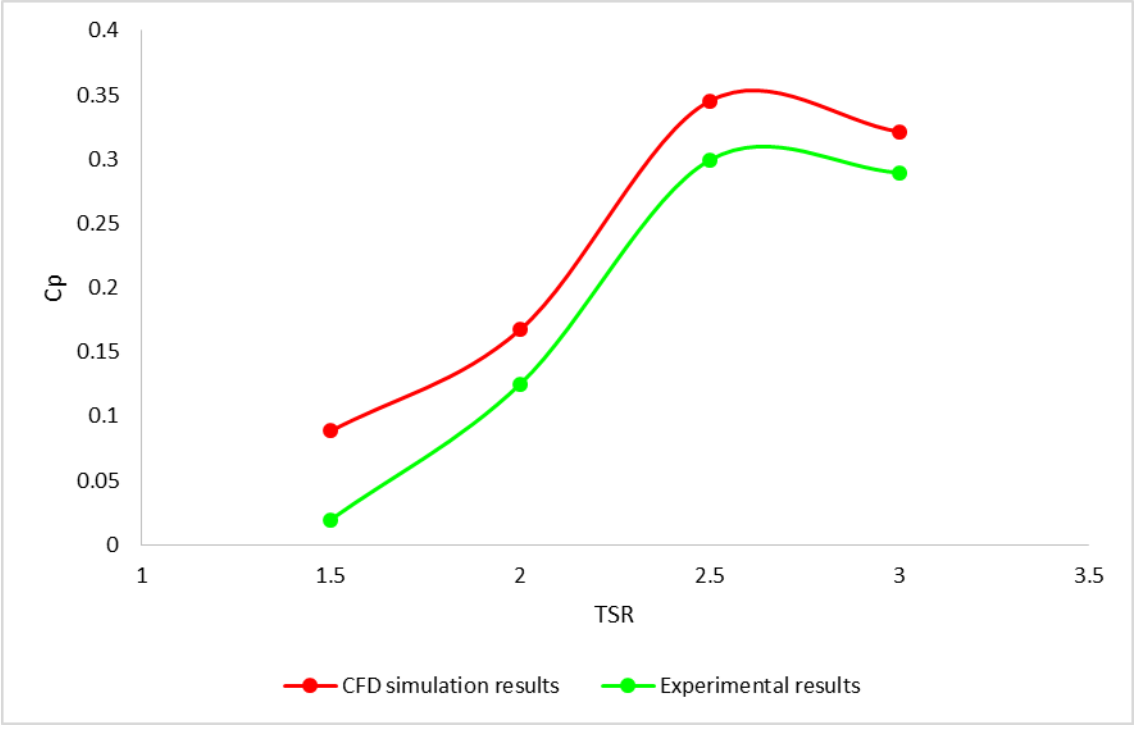

Fig. 4 Cp values from CFD simulation compared with the experimental study results.

As shown in Fig. 4, the CFD simulation results have an acceptable agreement with experimental results, and also, C_p values at TSR=2.5 have the highest amount in both studies; therefore, the CFD method is validated. The reason for the difference between the numerical and experimental results is the two-dimensionality of the solution and the neglect of mechanical losses due to the removal of arms and shafts, but these assumptions have been considered due to the reduction of computational costs. It should be noted that the Darrieus lift-base turbine does not have self-start capability, and the presence of mechanical equipment has caused the C_p values in initial TSRs to be insignificant. As a result, the difference between the numerical and experimental results has been more significant in the early TSRs. The error percentage in the last two TSRs was equal to 14% and 10%, respectively. The numerical solution is valid with the acceptable trend agreement of two CFD and experimental graphs and the percentage of errors obtained. A sensitivity and mesh independence analysis is performed for a single turbine as the next verification step, and the mesh is refined three times until no detectable change in rotor power coefficients is observed. The specifications of the grids applied in each refinement step and the important values related to them are given Table: 2. Also, for a better understanding of the grid independence, the overall torque values as a function of the azimuth angle for all three mesh cases in a complete rotation are given in Fig. 5.

Table: 2 Mesh study analysis

Value	Mesh 1(coarse)	Mesh 2(Medium)	Mesh 3(Fine)
Number of total elements	225380	398900	874200

Airfoil grid size [mm]	0.05	0.01	0.005
Inflation growth rate	1.2	1.1	1.09
Inflation layers	12	14	16
y+ average	0.81	0.62	0.41
Average aspect ratio	12.112	8.134	4.007
C_p	0.2175	0.2217	0.2164

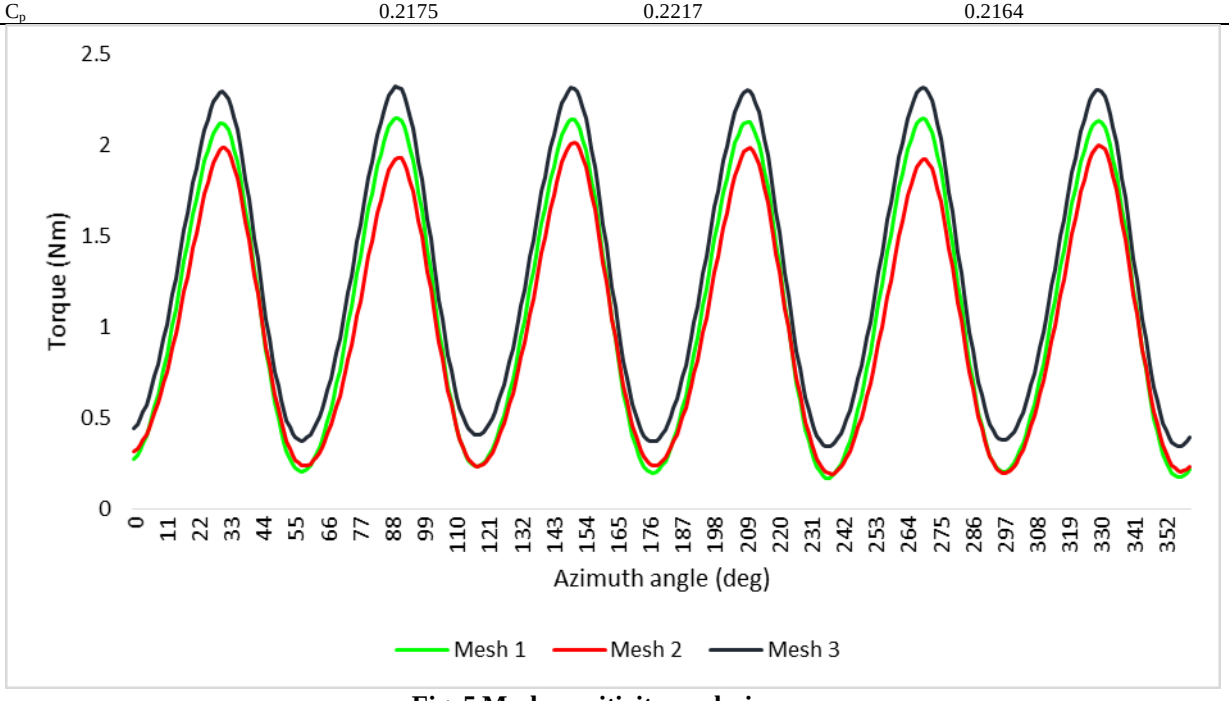

Fig. 5 Mesh sensitivity analysis.

According to Table: 2, the C_p value does not change significantly with the fineness of the mesh, and this shows the independence of CFD analysis from the number of mesh elements. The C_p value of the second and third mesh cases is less than one percent different from the first mesh case. Also, the values of y+ and aspect ratio are within an acceptable range. As a result, it can be claimed that the mesh has an acceptable quality. As for the Fig. 5 information, the overall torque in a complete rotation did not change significantly by mesh refining. The torque difference between the medium mesh and the coarse mesh case was 4% and 18% in the highest and lowest state, and the highest and lowest difference between the fine mesh and the coarse mesh was 10% and 19%; therefore, the solution is independent of mesh size and number.

6. Results and discussion

In this section, the installation distance of the turbines will be studied according to a particular pattern based on a factor of the rotor diameter. Then, considering the optimal distance for the rotor's rotational direction will be evaluated based on whether it is clockwise or counter clockwise to find a suitable pattern for the direction of rotation and optimum installation distance for V-shape and rhombus configuration layout for wind farm design.

6.1. Installation distance

By keeping constant the upstream turbine position, two same Darrieus VAWTs are placed in the mentioned different positions with different vertical and lateral distances at the downstream section in order to investigate the effect of the rotors installation distance on the overall C_p value of the wind farm. In the first step of the simulation, all three turbines, A, B, and C, are rotating counter-clockwise. In Table: 3, the calculated average C_p for each layout in a specified coordinate is demonstrated. The turbine cluster's average C_p value, which is illustrated in Table 3, is equal to the turbine A, B, and C average C_p. The average C_p of each VAWT cluster layout is compared to the single turbine average C_p value, which is equal to 0.2307.

According to Table: 3, VAWT 1 cluster configuration has a higher overall efficiency than other layouts. This means that it is higher than cases 2, 3, and 4 by 46.6, 50.5 and 54.5% respectively. As a result, based on the obtained average C_p values for each configuration, the optimum lateral and vertical distance for installing downstream VAWT rotors is equal to 1.5D; however, the average efficiency of all configurations is lower than the average efficiency of a single turbine; therefore, the motivation to investigate the rotor's direction of rotation in the 1.5D

lateral and vertical distance, increases in the next step. To more accurately investigate the downstream turbine's overall performance by growing the distance from the upstream turbine, a new parameter called distance is introduced, which is the considered distance from the center of downstream turbines to the center of the upstream turbine, which is equal to $\sqrt{x^2+y^2}$ The overall efficiency of VAWT clusters as a function of distance is shown in Fig. 6.

Table: 3 Power coefficient with varying turbine spacing

Layout	The center coordinate of two downstream turbines		C_p			Average C_p	Comparison with the single turbine average C_p
	$\|x\|$	$\|y\|$	Turbine A	Turbine B	Turbine C		
Case 1	1.5D	1.5D	0.2396	0.1696	0.1982	0.2025	-12.2%
Case 2	2D	2D	0.2074	0.0555	0.0611	0.1080	-53.2%
Case 3	2.5D	2.5D	0.1981	0.0515	0.0508	0.1001	-56.6%
Case 4	3D	3D	0.1944	0.0381	0.0442	0.0922	-60.1%

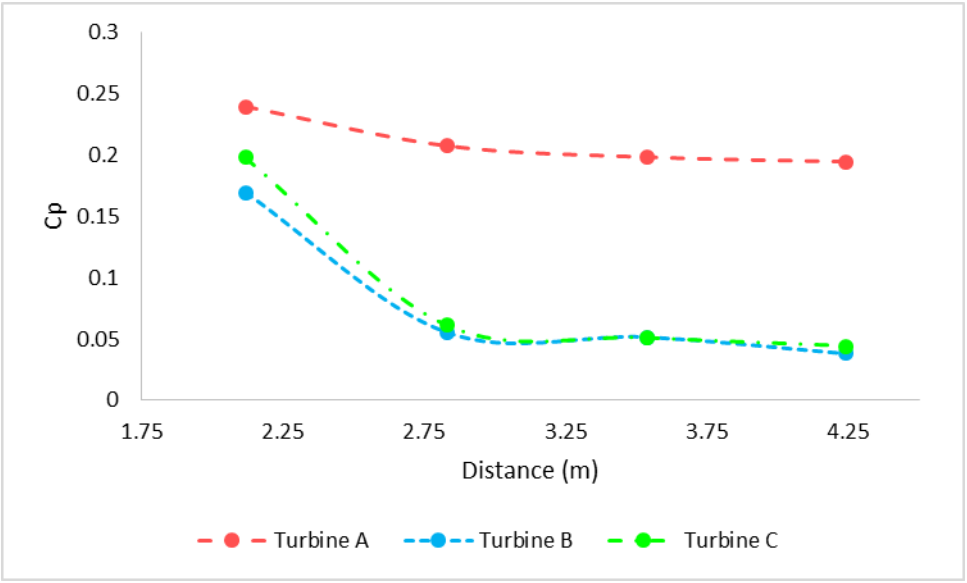

Fig. 6 Power coefficient as a function of turbine spacing for each turbine

Based on the information in Fig. 6, as the downstream turbine installation distance moves away from the upstream turbine center and the airflow inlet, the overall efficiency decreases remarkably. It is also clear that with the increase of the installation distance, the upstream turbine efficiency drop is negligible if all three turbines rotate counter-clockwise. In other words, when all three turbines rotate counter-clockwise, the upstream turbine does not receive significant influence from the downstream turbines. Finally, it is observed that the efficiency of turbine C is slightly higher than turbine B's efficiency. To show the main reason why the case1 configuration is optimal over the other cases, the velocity stream path line is given in Fig. 7.

According to Fig. 7, a favorable velocity gradient has been formed around the rotors, which makes an enhancement in the rotors' aerodynamic performance; it means the favorable velocity gradient can reduce the negative effects of wake flow formed in the downstream sections of rotors and around trailing edges. In case 1, when the rotors are placed at the closest possible installation distance, the interaction between the rotors is greater; therefore, it is possible to reuse the favorable velocity gradient for the adjacent rotors, and not only downstream rotors can reuse the favorable velocity gradient but also the negative impacts of wake flow is reduced significantly when rotors are closed to each other. If the rotors move away from each other, the possibility of reusing the favorable velocity gradient for the rotors is reduced, and the overall efficiency of the VAWT cluster is decreased

remarkably, and subsequently the negative effects of wake flow can make a reduction in downstream rotors. Reusing the favorable velocity gradient at closer installation distances has not only kept the downstream turbines' output power high but has also had a positive effect on the upstream turbine efficiency compared to farther distances. Also, at large distances, the possibility of growth of the stagnation zone due to the wake flow downstream of the rotors increases, which causes a decrease in overall C_p values. In general, large distances cause the distribution of the wake current, which reduces the speed and creates a stagnation zone around the rotors. To achieve the highest C_p and ensure optimum installation distance, the Kriging method, which is an optimization approach, has been employed to determine the optimum position for downstream turbines. This method optimizes the results with the help of DOE design by considering different distances in the form of various test scenarios. The optimization results are given in Fig. 8.

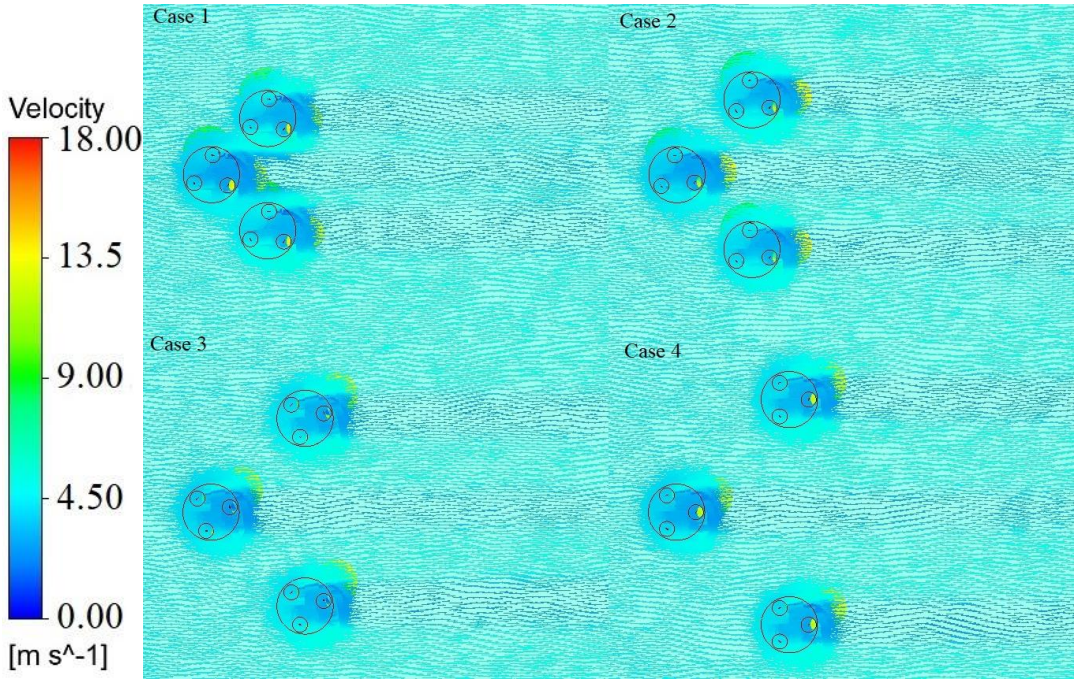

Fig. 7 Velocity stream path line for different installation distances.

The optimization results recommend and ensure 1.5D spacing for both lateral and vertical distances; as a result, 1.5D spacing is used to investigate the effect of the rotational direction on the upstream turbine performance and the VAWT cluster's overall efficiency.

6.2. Rotational direction

To investigate the effects of turbine rotational direction on the VAWT cluster efficiency, the optimized turbine cluster configuration (1.5D) has been studied in a different rotational direction combination. The upstream turbine direction of rotation has not changed and is still considered to be counter-clockwise. Due to the two downstream turbines, four different layouts are dependent on the rotational direction, as shown in Fig. 9. Except for the first case where all three rotors rotate counter-clockwise (CCW), the other three cases where both downstream turbines rotate clockwise (CW), and two other modes where one time turbine B is CW and another time for the next case turbine C is considered CW. It should be noted that the placement pattern of the blades changes depending on whether the rotors are CW or CCW, which means that the position of the leading edge and trailing edge are reversed to each other in two different rotational directions; therefore, the airflow direction on the blades is formed correctly.

Table: 4 illustrates the achieved average C_p for different combinations of clockwise (CW) or counter-clockwise (CCW) turbine B and turbine C rotational direction. The average C_p of each VAWT cluster combination is compared to the single turbine average C_p value, which is equal to 0.2307.

Based on the information in Table: 4, when turbine B rotates clockwise, in other words, it is counter-rotating two turbines, A and B, the efficiency of the upstream turbine and subsequently the overall C_p of the VAWT cluster

increases significantly. Meanwhile, when the two downstream turbines rotate clockwise and counter-rotating turbine A, the lowest efficiency is achieved for the VAWT cluster. As a result, the rotational direction of the downstream rotors, which changes the order of the leading edge and trailing edge, has caused a change in the overall C_p value of the upstream turbine. To better understand the improvement of the average efficiency of the upstream turbine and two downstream turbines in case 4 compared to the average efficiency of a single turbine, the results are compared in Fig. 10.

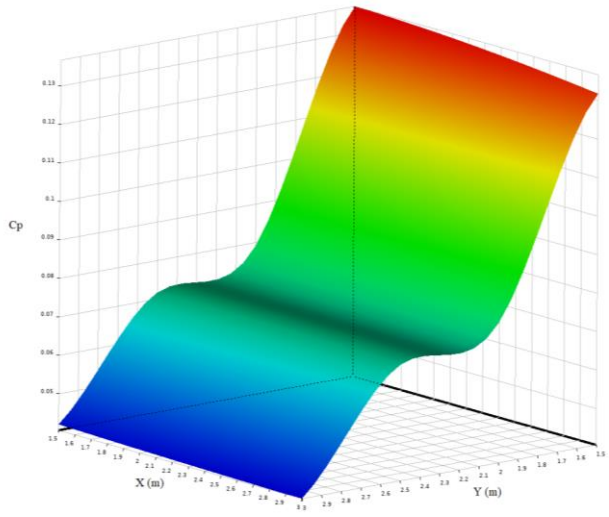

a

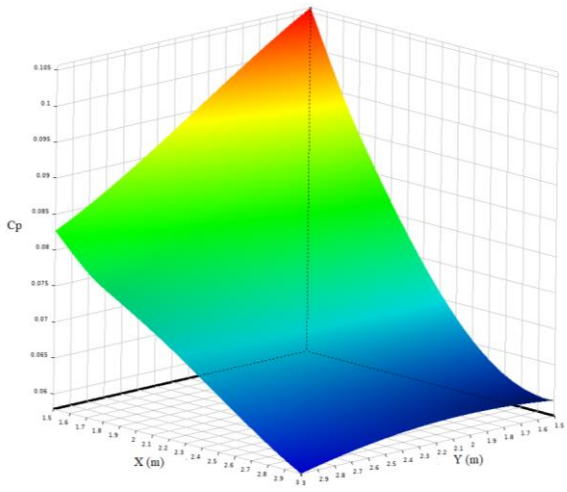

b

Fig. 8 a) Optimum distance for turbine B b) Optimum distance for turbine C.

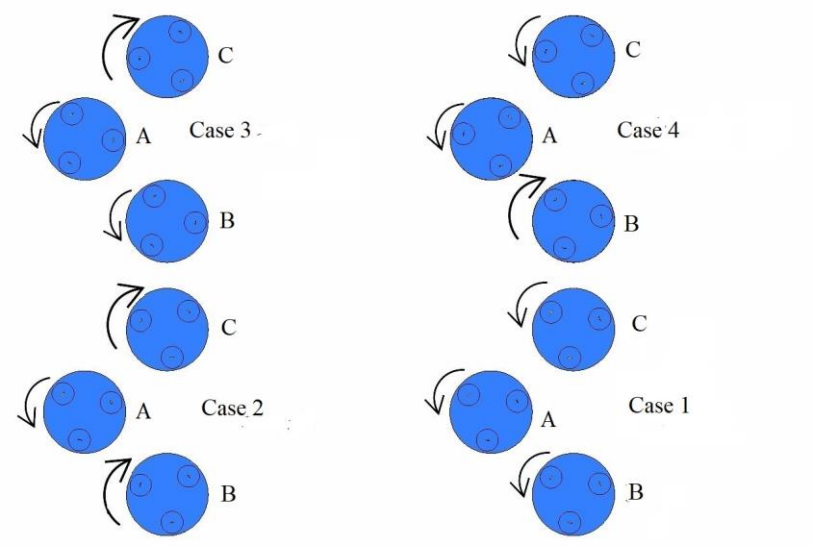

Fig. 9 Configuration of the turbine's cluster.

Table: 4 The average C_p for different rotational direction

Layout	Rotational direction			C_p			Average C_p	Comparison with the single turbine average C_p
	Turbine A	Turbine B	Turbine C	Turbine A	Turbine B	Turbine C		
Case 1	CCW	CCW	CCW	0.2396	0.1696	0.1982	0.2025	-12.2%
Case 2	CCW	CW	CW	0.1637	0.0799	0.0956	0.1131	-50.9%
Case 3	CCW	CCW	CW	0.2371	0.1107	0.1267	0.1581	-31.5%
Case 4	CCW	CW	CCW	0.5049	0.3241	0.3271	0.3854	+67.1%

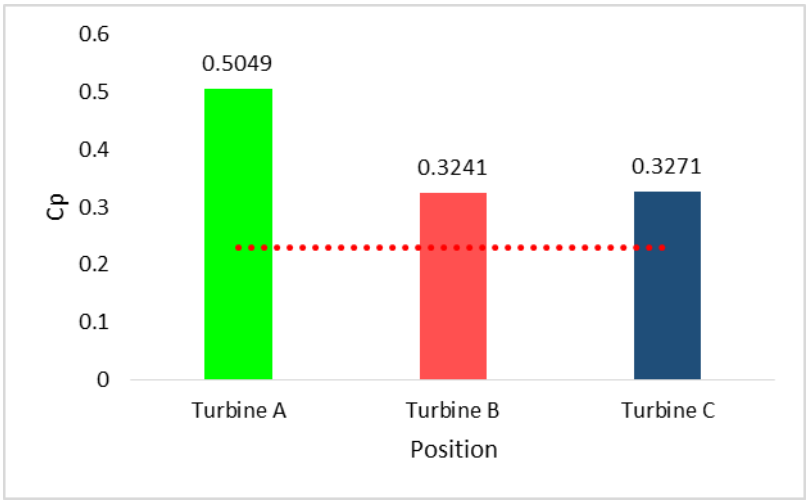

Fig. 10 Comparison of average C_p values for each turbine in optimum turbine rotational direction

As for the Fig. 10 information, the average efficiency of turbines A, B, and C in case 4 configuration, which is the optimal rotor rotational direction, has increased by 118%, 40%, and 42%, respectively, from the average C_p

value of the single turbine, which was 0.2307. Fig. 11 illustrates the velocity stream path line for different rotational directions.

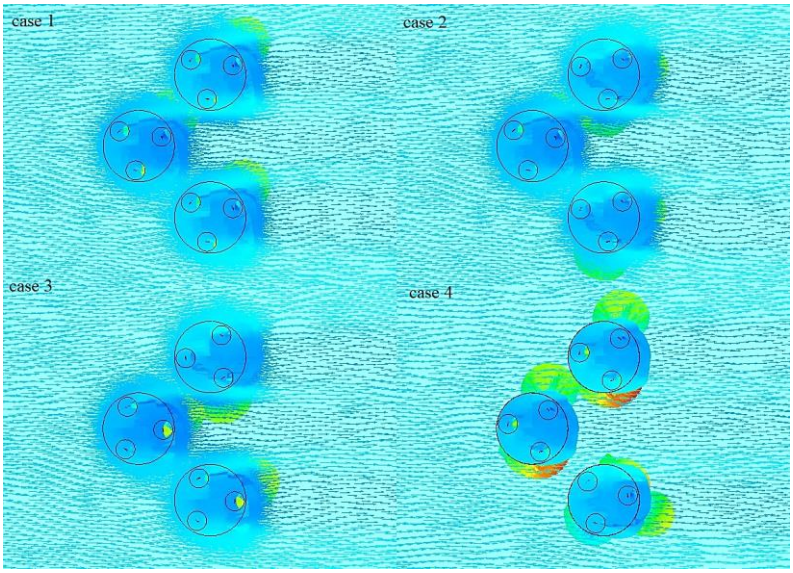

Fig. 11 Velocity stream path line for different rotational directions

Regarding Fig. 11, case 4, when turbine B is rotating clockwise, the favorable velocity gradient can be seen around the rotors and blades, and the velocity stagnation zone between the rotors and blades is not intense, which indicates the effective airflow between the rotors, resulting in higher overall efficiency. In case 2, where both downstream turbines are assumed to be clockwise, strong wake flow at the rotors downstream section is evident, resulting in a significant drop in the favorable velocity gradient between the rotors and the blades and subsequently causing the dominant velocity stagnation zone in these areas which led to a decrease in overall efficiency. As a result, the direction of rotation of Darrieus rotors changing the geometry of the blades and placing the leading edge and trailing edge in the order corresponding to CW or CCW of the rotors leads to more effective airflow between the blades and rotors.

6.3. Multiple VAWTs cluster

The main objective of this section is to evaluate the cluster configuration of VAWTs in order to model a wind farm. In this section, two configuration models were studied; the first is the normal V-shaped configuration, including five and seven turbines, and the second is the rhombic configuration, including four, eight, and twelve Darrieus VAWTs. It is noteworthy that the lower downstream turbines in both V-shaped and rhombic models are counter-rotating with the reference leading rotor and the upper downstream rotors and their rotational direction is considered clockwise. In both configurations, the upper downstream turbines and leading turbines are co-rotating, and their direction of rotation is counter-clockwise. The reason for this assumption is following the previous section results, as it was found that the highest overall efficiency is when the downstream turbine is counter-rotating with the leading turbine and clockwise. Fig. 12 shows both V-shaped and rhombic configurations.

The overall C_p of all present turbines in six different v-shaped and rhomboidal configurations compared to the single turbine is given in Fig. 13.

From the bar chart, it is clear that in all different configurations, the leading turbine (turbine A) overall efficiency is significantly higher than the single turbine case, which means the downstream turbines have a positive impact on the leading turbine efficiency. Turbine A's overall C_p is 54%, 34%, 34%, 38%, 37%, and 36% in three, five, and seven V-shape configurations and four, eight, and twelve rhombic configurations higher than single turbine overall C_p value respectively. In addition, the overall C_p of turbine C in all three, five, and seven V-shaped configurations is 29%, 17%, and 16% higher than the overall single turbine C_p value, while the overall efficiency of turbine B is only 28% higher in the three-turbine V-shaped configuration than the single turbine case. Meanwhile, the overall efficiency of other rotors separately in both V-shaped and rhombic configurations is lower than the single turbine's overall efficiency. To better understand the reason for the decrease or increase in the $C_p$value of the rotors in different layouts, the velocity stream path line for both V-shaped and rhombic configurations is given in Fig. 14.

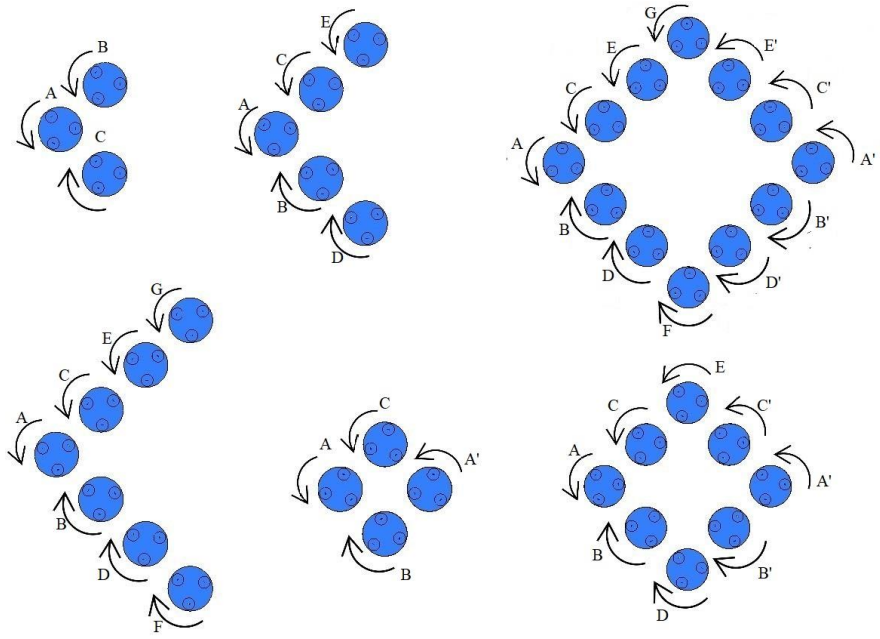

Fig. 12 V-shaped and rhombic configurations.

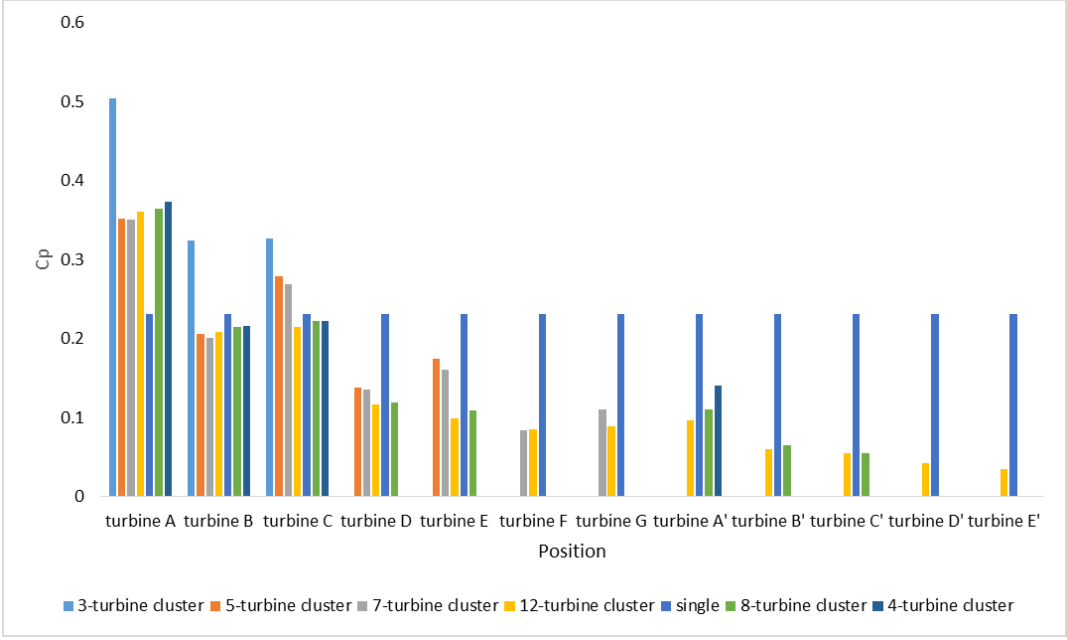

Fig. 13 Power coefficient of each turbine for different cluster

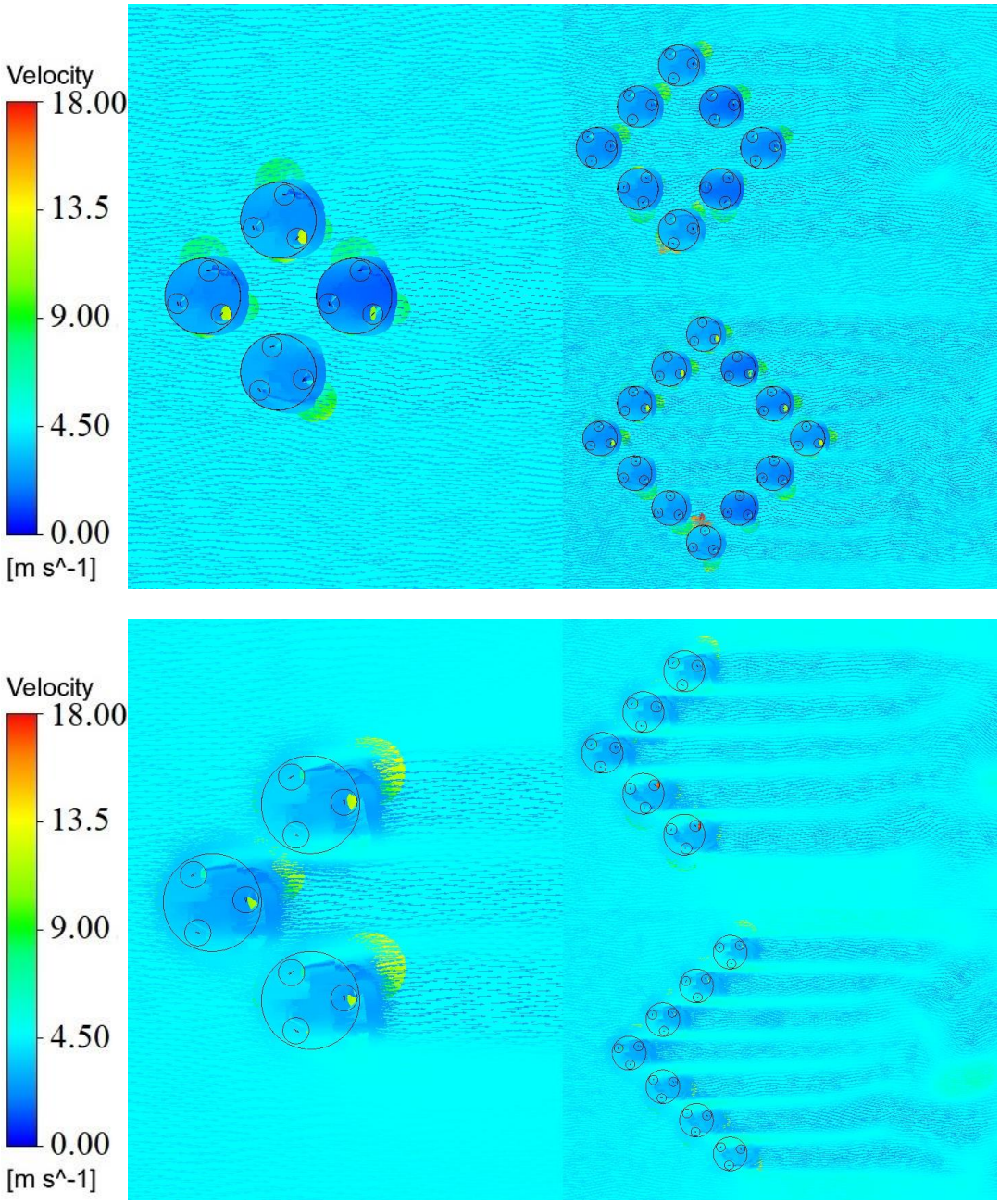

Fig. 14 Velocity stream path line for both V-shaped and rhombic layouts

Based on Fig. 14, in the downstream section of rotors number A to G in the V-shaped arrangement, a strong wake flow regime has been formed, which continues to the rear rotor's position in a rhombic arrangement, and this phenomenon causes the velocity stagnation zone between the rear rotors' blades (A' to E'). It is obvious that the velocity stagnation zone causes a reduction in the overall efficiency of rear rotors in rhombic configuration. The velocity stagnation zone between the rear turbine blades is much more intense than in normal situation and due to the positive velocity gradient around the rotors, it can cause lift force imbalance, which imposes a local stall in the rear rotor blades in the rhombic configuration; however, the observations showed that mentioned local stall occurs instantly and the favorable velocity gradient recovered rear rotors performance. It can also be claimed that the intensity of the wake flow between the blades of the rotors A' to E' is very high, and the reason is that the wake flow caused by the turbines A to G did not exit the wind farm and was trapped in the limited area. The inconvenient confinement of the wake flow, which has a velocity close to zero, in the limited space in the rhombus configuration

has caused this flow to be absorbed by the rear turbines and, ultimately, the overall power reduction. In the rhombic configuration, in the arrangement of 4 turbines, rotor A', in the arrangement of 8 turbines, rotors B' and C,' and in the arrangement of 12 turbines, rotors D' and E,' which were at the closest distance to the leading turbines, most affected by the destructive trapped wake flow.

7. Conclusion

In this study, a Darrieus VAWT model was selected as a CFD analysis sample, and after validation and mesh independence study, the CFD investigation was conducted on a wind farm consisting of similar Darrieus VAWT clusters. The simulation was conducted to find the best installation distance and rotational direction of the rotors, and the optimal case was applied to two different V-shaped and rhombic configurations. A results summary is as follows.

- Four installation distances, 1.5D, 2D, 2.5D, and 3D, were investigated and the results showed that with an excessive increase in the downstream turbine installation distance, the overall efficiency decreases significantly, and the CFD results and optimization using the Kriging method ensured that 1.5D installation distance has been the optimum case.
- At the optimal installation distance of 1.5D, four different rotational directions were investigated and it was found that the best condition occurs when the lower downstream turbine works in the clockwise direction and was counter-rotation with the other two rotors.
- Two different configurations were investigated. V-shaped layout with three, five, and seven turbines and rhombus arrangement with four, eight, and twelve turbines. The results showed that the rear turbines' overall efficiency in the rhombus layout was strongly influenced by the front turbines' wake flow and their efficiency decreased. However, turbine A is affected by downstream turbines and has a higher overall efficiency than a single turbine in all configurations.

References

[1] S. L. Dixon, C. A. Hall, ScienceDirect, 2014, *Fluid mechanics and thermodynamics of turbomachinery*, Butterworth-Heinemann, Amsterdam, Seventh edition.ed.

[2] A. M. Abusorrah, F. Mebarek-Oudina, A. Ahmadian, D. Baleanu, Modeling of a MED-TVC desalination system by considering the effects of nanoparticles: energetic and exergetic analysis, *Journal of Thermal Analysis and Calorimetry*, Vol. 144, No. 6, pp. 2675-2687, 2021.

[3] B. Hand, A. Cashman, A review on the historical development of the lift-type vertical axis wind turbine: From onshore to offshore floating application, *Sustainable Energy Technologies and Assessments*, Vol. 38, 2020.

[4] M. K. Johari, M. Jalil, M. Shariff, Comparison of horizontal axis wind turbine (HAWT) and vertical axis wind turbine (VAWT), Vol. 7, pp. 74-80, 10/09, 2018.

[5] A. Abjadi, F. Ghafoorian, S. Chegini, Effect of Nozzle Installation on The Aerodynamic Performance of A Savonius Vertical Axis Wind Turbine, Using CFD method, *Journal of Mechanical Research and Application*, Vol. 11, No. 4, pp. 87-70, 2022. en

[6] M. Moghimi, H. Motawej, Investigation of Effective Parameters on Gorlov Vertical Axis Wind Turbine, *Fluid Dynamics*, Vol. 55, No. 3, pp. 345-363, 2020.

[7] M. Ahmad, A. Shahzad, F. Akram, F. Ahmad, S. I. A. Shah, Design optimization of Double-Darrieus hybrid vertical axis wind turbine, *Ocean Engineering*, Vol. 254, pp. 111171, 2022/06/15/, 2022.

[8] N. E. Chowdhury, M. A. Shakib, F. Xu, S. Salehin, M. R. Islam, A. A. Bhuiyan, Adverse environmental impacts of wind farm installations and alternative research pathways to their mitigation, *Cleaner Engineering and Technology*, Vol. 7, pp. 100415, 2022/04/01/, 2022.

[9] H. Abdelkader, F. Mebarek-Oudina, D. Belatrache, 2022, *Renewable Energy Technologies: Research Methods and Applications*,

[10] M. Sawant, S. Thakare, A. P. Rao, A. E. Feijóo-Lorenzo, N. D. Bokde, A Review on State-of-the-Art Reviews in Wind-Turbine- and Wind-Farm-Related Topics, *Energies*, Vol. 14, No. 8, pp. 2041, 2021/04/07/, 2021. en

[11] W. Zuo, X. Wang, S. Kang, Numerical simulations on the wake effect of H-type vertical axis wind turbines, *Energy*, Vol. 106, pp. 691-700, 2016.

[12] T. Uchida, Y. Taniyama, Y. Fukatani, M. Nakano, Z. Bai, T. Yoshida, M. Inui, A New Wind Turbine CFD Modeling Method Based on a Porous Disk Approach for Practical Wind Farm Design, *Energies*, Vol. 13, No. 12, pp. 3197, 2020/06/19/, 2020. en

[13] S. Shaaban, A. Albatal, M. H. Mohamed, Optimization of H-Rotor Darrieus turbines' mutual interaction in staggered arrangements, *Renewable Energy*, Vol. 125, pp. 87-99, 2018/09//, 2018. en

[14] J. Chen, Y. Zhang, Z. Xu, C. Li, Flow characteristics analysis and power comparison for two novel types of vertically staggered wind farms, *Energy*, Vol. 263, pp. 126141, 2023/01/15/, 2023.

[15] B. Zhang, B. Song, Z. Mao, W. Tian, A novel wake energy reuse method to optimize the layout for Savonius-type vertical axis wind turbines, *Energy*, Vol. 121, pp. 341-355, 2017/02//, 2017. en

[16] L. N. Azadani, Vertical axis wind turbines in cluster configurations, *Ocean Engineering*, Vol. 272, pp. 113855, 2023/03/15/, 2023.

[17] H. Su, H. Meng, T. Qu, L. Lei, Wind tunnel experiment on the influence of array configuration on the power performance of vertical axis wind turbines, *Energy Conversion and Management*, Vol. 241, pp. 114299, 2021/08//, 2021. en

[18] J. E. Silva, L. A. M. Danao, Varying VAWT Cluster Configuration and the Effect on Individual Rotor and Overall Cluster Performance, *Energies*, Vol. 14, No. 6, pp. 1567, 2021/03/12/, 2021. en

[19] M. Torresi, B. Fortunato, S. M. Camporeale, An Efficient 3D CFD Model for the Analysis of the Flow Field Around Darrieus Rotors, in *Proceeding of Volume 8: Supercritical CO2 Power Cycles; Wind Energy; Honors and Awards*, San Antonio, Texas, USA: American Society of Mechanical Engineers, pp. V008T44A020. en

[20] J. O. Dabiri, Potential order-of-magnitude enhancement of wind farm power density via counter-rotating vertical-axis wind turbine arrays, *Journal of Renewable and Sustainable Energy*, Vol. 3, No. 4, pp. 043104, 2011/07//, 2011. en

[21] A. Vergaerde, T. D. Troyer, S. Muggiasca, I. Bayati, M. Belloli, M. C. Runacres, Influence of the direction of rotation on the wake characteristics of closely spaced counter-rotating vertical-axis wind turbines, *Journal of Physics: Conference Series*, Vol. 1618, No. 6, pp. 062017, 2020/09/01/, 2020. en

[22] Y. Zheng, H. L. Bai, C. M. Chan, Optimization of Savonius turbine clusters using an evolutionary based Genetic Algorithm, *Innovative Solutions for Energy Transitions*, Vol. 158, pp. 637-642, 2019/02/01/, 2019.

[23] Y. A. Al-Turki, F. Mebarek-Oudina, A. Ahmadian, D. Baleanu, Flat sheet direct contact membrane distillation desalination system using temperature-dependent correlations: thermal efficiency via a multi-parameter sensitivity analysis based on Monte Carlo method, *Journal of Thermal Analysis and Calorimetry*, Vol. 144, No. 6, pp. 2641-2652, 2021.

[24] S. Ahmad, S. Mehfuz, F. Mebarek-Oudina, J. Beg, RSM analysis based cloud access security broker: a systematic literature review, *Cluster Comput*, Vol. 25, No. 5, pp. 3733-3763, 2022.

[25] M. Akhlagi, F. Ghafoorian, M. Mehrpooya, M. Sharifi Rizi, Effective Parameters Optimization of a Small Scale Gorlov Wind Turbine, Using CFD Method, *Iranian Journal of Chemistry and Chemical Engineering*, 2022. en

[26] M. Raciti Castelli, G. Ardizzon, L. Battisti, E. Benini, G. Pavesi, Modeling Strategy and Numerical Validation for a Darrieus Vertical Axis Micro-Wind Turbine, 2010, pp. 409-418.

[27] S. Chegini, F. Ghafoorian, M. Moghimi, M. Mehrpooya, Optimized arrangement of clustered Savonius VAWTs, Techno-Economic evaluation and feasibility of installation, *Iranian Journal of Chemistry and Chemical Engineering*, 2023. en

[28] M. Asadbeigi, F. Ghafoorian, M. Mehrpooya, S. Chegini, A. Jarrahian, A 3D Study of the Darrieus Wind Turbine with Auxiliary Blades and Economic Analysis Based on an Optimal Design from a Parametric Investigation, *Sustainability*, 15, 2023].

[29] M. Mehrpooya, M. Asadbeigi, F. Ghafoorian, S. Farajyar, Investigation and Optimization on Effective Parameters of a H-rotor Darrieus Wind Turbine, Using CFD Method, *Iranian Journal of Chemistry and Chemical Engineering*, 2023. en

[30] R. Nichols, 2010, *Turbulence Models and Their Application to Complex Flows*,

[31] M. Akhlaghi, F. Ghafoorian, Investigation of Arc Angle Rotor Blade Variations Effect of Savonius Vertical Axis Wind Turbine on Power and Torque Coefficients Using a 3D Modeling, *Renewable Energy Research and Applications*, Vol. 4, No. 1, pp. 13-19, 2023. en

[32] C. Sun, B. Song, P. Wang, Parametric geometric model and shape optimization of an underwater glider with blended-wing-body, *International Journal of Naval Architecture and Ocean Engineering*, Vol. 7, No. 6, pp. 995-1006, 2015/11/01/, 2015.